Information content of aerosol retrievals in the sunglint region

M. Ottaviani,[1,2] K. Knobelspiesse,[1,3] B. Cairns,[1] and M. Mishchenko[1]

[1] We exploit quantitative metrics to investigate the information content in retrievals of atmospheric aerosol parameters (with a focus on single-scattering albedo), contained in multi-angle and multi-spectral measurements with sufficient dynamical range in the sunglint region. The simulations are performed for two classes of maritime aerosols with optical and microphysical properties compiled from measurements of the Aerosol Robotic Network. The information content is assessed using the inverse formalism and is compared to that deriving from observations not affected by sunglint. We find that there indeed is additional information in measurements containing sunglint, not just for single-scattering albedo, but also for aerosol optical thickness and the complex refractive index of the fine aerosol size mode, although the amount of additional information varies with aerosol type. **Citation:** Ottaviani, M., K. Knobelspiesse, B. Cairns, and M. Mishchenko (2013), Information content of aerosol retrievals in the sunglint region, *Geophys. Res. Lett.*, *40*, 631–634, doi:10.1002/grl.50148.

1. Introduction

[2] While the radiative forcings exerted by some atmospheric constituents (such as greenhouse gases) are known with satisfactory accuracy, the role of aerosols bears uncertainties so large that they prevent climate models from running at the desirable accuracy [*Hansen et al.*, 2011; *Penner et al.*, 2011; *Loeb and Su*, 2010]. The impact of aerosol particulates is indeed complex and includes both direct and indirect effects, leading to positive and negative forcings via a myriad of feedback mechanisms. Direct effects are mostly determined by the microphysical properties, which govern the ratio between absorption (leading to positive feedback or warming) and scattering (leading to cooling when radiation is reflected back to space) of electromagnetic radiation. Highly reflecting sulfate aerosols can originate from volcanic eruptions [*Bates et al.*, 1992] and fossil fuel combustion [*Smith et al.*, 2001] or within the silicates which predominantly contribute to the composition of dust raised by sandstorms [*Wagner et al.*, 2012]. Carbonaceous particulates, originating from biomass, biofuel, and fossil fuel burning, are characterized instead by non-negligible absorption [*Moosmüller et al.*, 2009], and much emphasis has recently been placed on the uncertainty associated with the efficiency of this specific process [*Andreae*, 2001].

[3] The parameters of importance in aerosol retrieval are the column optical thickness, the effective radius and variance, and the complex refractive index. The typical bimodal nature of aerosol populations requires these parameters to be determined for both modes. The overall situation is further complicated by the extensive variability of aerosol distribution, deriving from regional emission sources and from the vertical assortment linked to the dynamics of transport processes [*Seinfeld et al.*, 1998].

[4] A decade ago, *Kaufman et al.* [2002] hypothesized that sunglint, the strong signal caused by reflection of sunlight from water surfaces, could be exploited to improve the retrievals of aerosol absorption. The strategy envisioned the exploitation of off-glint regions to constrain the scattering properties of the aerosol, especially feasible if polarimetric measurements are available [*Mishchenko and Travis*, 1997], together with direct transmittance measurements at the center of the glint, where the higher signal-to-noise ratio would arguably benefit the estimate of extinction. Despite the efforts to improve the description of the sunglint phenomenon [*Kay et al.*, 2009], and include it in radiative transfer codes as a boundary condition [*Ottaviani et al.*, 2008], a rigorous assessment of the feasibility of improved retrievals in glint regions is still missing. Because of this, and the lack of sufficient dynamical range, a wealth of satellite observations is systematically discarded. A clear example concerns the ocean color community, since each composite image of global chlorophyll concentration exhibits periodic, wide latitudinal swaths of missing data.

[5] Inverse methods are most general and can be applied to the widest class of retrievals. Well-established inversion schemes [*Rodgers*, 2000], to predict the uncertainty of parameters retrieved from an observation of given characteristics (spectral range, radiometric uncertainty, etc.), have been used to test the retrieval capability of multi-angle, multi- and hyperspectral, and polarimetric instruments [*Rodgers and Connor*, 2003; *Lebsock et al.*, 2007; *Hasekamp and Landgraf*, 2007; *Waquet et al.*, 2009; *Hasekamp*, 2010; *Knobelspiesse et al.*, 2011; *Coddington et al.*, 2012]. Adhering to the implementation of *Knobelspiesse et al.* [2012], who compared contemporary instrument designs for the retrieval of fine mode aerosol properties, we investigate the potential value of measurements taken within the sunglint region.

2. Methodology

[6] The act of measurement always introduces some noise $\boldsymbol{\epsilon}$ in the relation linking the *n*-dimensional *state vector* of a system $\mathbf{x}$ to an *m*-dimensional *measurement vector* $\mathbf{y} = \mathbf{F}(\mathbf{x}) + \boldsymbol{\epsilon}$, where $\mathbf{F}$ is the *forward model* which describes the knowledge of the measurement process and the physics of the problem (which may be imperfect). The forward model can often be locally linearized about a reference state $\mathbf{x}_0$:

[1]NASA Goddard Institute for Space Studies, New York, New York, USA.
[2]Stevens Institute of Technology, Hoboken, New Jersey, USA.
[3]NASA Postdoctoral Program, Oak Ridge, Tennessee, USA.

Corresponding author: M. Ottaviani, NASA Goddard Institute for Space Studies, New York, NY, USA. (mottavia@stevens.edu)

$$\mathbf{y} - \mathbf{F}(\mathbf{x}_0) = \frac{\partial \mathbf{F}(\mathbf{x})}{\partial \mathbf{x}}(\mathbf{x} - \mathbf{x}_0) + \boldsymbol{\epsilon} = \mathbf{K}(\mathbf{x} - \mathbf{x}_0) + \boldsymbol{\epsilon} \quad , \quad (1)$$

with the $m \times n$ *Jacobian* matrix $K_{ij} = \partial F_i(\mathbf{x})/\partial x_j$ expressing the sensitivity of the model to an infinitesimal change in each parameter. Each of the m rows of $\mathbf{K}$ corresponds (i.e., maps) to a coordinate in measurement space.

[7] To know how a measurement updates a certain prior knowledge $P(\mathbf{x})$ of a state, we can use Bayes' theorem which provides information on how the measurement *probability density function* (pdf) maps into state space and combines with the a-priori pdf to form an a-posteriori pdf $P(\mathbf{x}|\mathbf{y})$ for the state: $P(\mathbf{x}|\mathbf{y}) = P(\mathbf{y}|\mathbf{x})P(\mathbf{x})/P(\mathbf{y})$. The probability $P(\mathbf{y}|\mathbf{x})$, of obtaining $\mathbf{y}$ if the state is $\mathbf{x}$, is described by the statistics of the measurement noise since $\mathbf{x}$ is mapped into the region of measurement space enclosed by the measurement error. $P(\mathbf{y})$ is often disregarded as a normalization factor. For linear problems with Gaussian statistics, Bayes' theorem enables the derivation of expressions for the expected value $\hat{\mathbf{x}}$ of the state vector and for the associated $n \times n$, *retrieval error* covariance matrix $\hat{\mathbf{S}}$:

$$\hat{\mathbf{x}} = \mathbf{x}_a + \left(\mathbf{K}^T \mathbf{S}_\epsilon^{-1} \mathbf{K} + \mathbf{S}_a^{-1}\right)^{-1} \mathbf{K}^T \mathbf{S}_\epsilon^{-1}(\mathbf{y} - \mathbf{K}\mathbf{x}_a) \quad , \quad (2)$$

$$\hat{\mathbf{S}}^{-1} = \mathbf{K}^T \mathbf{S}_\epsilon^{-1} \mathbf{K} + \mathbf{S}_a^{-1} \quad (3)$$

with the superscript "–1" indicating the matrix inverse and "T" the matrix transpose. Equation (3) expresses the connection between instrument characteristics and retrieval uncertainty. The $m \times m$, symmetric and non-negative *measurement error* covariance matrix $\mathbf{S}_\epsilon$ describes the uncertainties associated with each measurement and their correlations. The $n \times n$, *a-priori error* covariance matrix $\mathbf{S}_a$ measures the uncertainties in $\mathbf{x}_a$, a guess of the state prior to making the measurement. Ultimately, the minimum of the *cost function* $\chi^2 = (\mathbf{y} - \mathbf{K}\mathbf{x})^T \mathbf{S}_\epsilon^{-1}(\mathbf{y} - \mathbf{K}\mathbf{x}) + (\mathbf{x} - \mathbf{x}_a)^T \mathbf{S}_a^{-1}(\mathbf{x} - \mathbf{x}_a)$ is found at $\hat{\mathbf{x}}$, where the expected value of χ^2 should be equal to the number of degrees of freedom m if the model is valid. When a-priori information is absent, the expression reduces to that for a weighted least squares regression.

[8] The Shannon information content (SIC), $H = -\frac{1}{2}\log_2 \left|\mathbf{S}^{-1}\mathbf{S}_a\right|$ where $|\cdot|$ is the determinant, is readily available once the covariance matrices are computed. This quantity expresses the gain of knowledge in bits of information consequent to the act of measurement, and it bears strict analogy with the thermodynamic definition of entropy. In state space, it measures the reduction of the volume enclosing the accessible states due to the observation.

[9] The simulations in this study were devised for a hypothetical instrument that can be considered as a common denominator among those already available in orbit. We examined along-track measurements of total reflectance only, at seven viewing angles as available with the Multi-angle Imaging Spectral Radiometer (MISR; [*Diner et al.*, 1998]) and the Polarization and Directionality of the Earth's Reflectances (POLDER; [*Tanré et al.*, 2011]). The MISR sensor has actually nine cameras, but observations at $\pm 70°$ were excluded because of concerns that vertical structure could create ambiguities at such shallow geometries. We also limited the number of available wavelengths to five channels in the visible (410, 440, 560, 670, and 870 nm) as POLDER and MISR do not have channels in the Short-Wave Infrared (SWIR).

[10] The resulting measurement vector contains a set of radiance measurements R_I made at various viewing angles θ_i for each spectral channel λ_i, $\mathbf{y} = \{R_I(\theta_1, \lambda_1), \ldots, R_I(\theta_m, \lambda_m)\}$. It is advantageous to use dimensionless reflectance units to keep the signal from different channels on the same scale. The relationship to intensity I is $R_I = (I\pi r_0^2)/(F_0 \cos\theta_s)$, where r_0 is the solar distance in astronomical units used to obtain the proper irradiance from the annual average exoatmospheric irradiance F_0 (W m^{-2}), and θ_s is the solar zenith angle. The measurement uncertainty associated with each R_I is composed of the instrument dark current noise σ_f, the *shot noise* σ_a, and the calibration uncertainty σ_b:

$$\sigma_{R_I}^2 = 2\sigma_f^2(R_I/I)^2 + \sigma_a(R_I/I) + \sigma_b^2 R_I^2 \quad . \quad (4)$$

[11] In this work, we assume a standardized model of instrumental uncertainty [*Knobelspiesse et al.*, 2012] with $\sigma_f = 7 \times 10^{-5}$, $\sigma_a = 7 \times 10^{-8}$, and $\sigma_b = 0.03$.

[12] Equation (4) defines the diagonal elements $S_{\epsilon,i,j} = (\sigma_{R_I}^2)i$ (for $i = j$). Uncertainties due to dark current and shot noise are assumed to be random, and thus uncorrelated. A description of angle-to-angle correlation in calibration errors, normally neglected for simplicity, is attempted as in *Knobelspiesse et al.* [2012] with a Markov process generating off-diagonal elements with the form:

$$\begin{aligned} S_{\epsilon,i,j} &= \sigma_b^2 (\sigma_{R_I})_i (\sigma_{R_I})_j \rho^{|a(i-j)|} & i \neq j, \text{ same channel,} \\ S_{\epsilon,i,j} &= 0 & i \neq j, \text{ different channels,} \end{aligned} \quad (5)$$

where a is the angular separation between adjacent, instantaneous fields of view in one scan, and ρ is a correlation parameter ranging from $\rho = 0$ (totally uncorrelated system) to $\rho = 1$ (fully correlated system). Here, we assumed $\rho = 0.9$ to represent the high angular correlation typical of calibration errors.

[13] The forward engine at the core of the procedure is based on the doubling-adding method [*De Haan et al.*, 1987]. The linearization process is repeated for eight different aerosol optical thicknesses (AOTs) between 0.039 and 1.0 at 560 nm in order to cover a large portion of the space of plausible aerosol loads. For each AOT, the Jacobians are estimated as finite derivatives via perturbing each state parameter x_j by a small amount. From the widely used suite compiled by *Dubovik et al.* [2002], and based on the large statistical sample of AErosol RObotic NETwork (AERONET; [*Holben et al.*, 1998]) observations, we selected two aerosol classes representative of a maritime scenario (see Table 1): the non-absorbing Lanai (LH) type, for which the AOT is equally partitioned between fine and coarse modes, and the moderately absorbing Maldives (MI) type, for which the fine mode is responsible for 90% of the AOT and the coarse mode for the remaining 10%. The aerosols are assumed to consist of homogenous spheres and are placed in the first kilometer of a parallel-slab atmosphere to mimic a

Table 1. Aerosol Microphysical Properties Used in This Study[a]

	Maldives	Lanai, HI
Refractive index	1.44–0.0110i	1.36–0.0015i
$r_{eff,f}$ (μm), $v_{eff,f}$	0.222, 0.236	0.201, 0.259
$r_{eff,c}$ (μm), $v_{eff,c}$	4.96, 0.782	4.29, 0.588
AOT$_f$(560 nm)/AOT$_{tot}$(560 nm)	0.9	0.5

[a]From the AERONET climatology in *Dubovik et al.* [2002]. The spherical, homogenous particles have a spectrally invariant refractive index. Size is specified bimodally with lognormal distributions.

standard boundary layer. The climatology of all aerosol classes is the a-priori knowledge used to compile the matrix $\mathbf{S}_a$.

[14] As with virtually every radiative transfer code capable of including a rough ocean as a lower boundary condition, we employ the model by *Cox and Munk* [1956], which parameterizes the wave slope distribution as a linear function of wind speed. The simulations were run for a solar zenith angle of $45°$ and a low wind speed ($3\,\mathrm{m\,s^{-1}}$) so that the glint is bright and limited in extent. This allows us to consider, as a first scene, scanning observations taking place along the principal plane of reflection where the sunglint signal reaches its peak. The second scene can then be selected at a relative azimuth of $30°$, where sunglint is nearly absent and the range of available viewing angles (which for scanners depends on the orientation relative to the principal plane) is only moderately affected. The underwater portion of light scattering was modeled with a value of chlorophyll *a* concentration of $0.1\,\mathrm{mg\,m^{-1}}$, representative of standard open-ocean waters [*Chowdhary et al.*, 2012].

3. Results and Discussion

[15] The absolute uncertainties as a function of AOT associated with retrievals from in-glint observations are depicted in Figure 1 with orange lines, and those from off-glint observations with blue lines. The solid and dashed line styles are for the MI and LH aerosol types, respectively. The values in the top-right corner of each panel represent the starting (a-priori)

value for the specific parameter: uncertainties remaining close to this initial choice are indicative of poor retrieval capabilities for the associated quantity. This kind of behavior is shown, for example, by the effective variance of the fine mode, which is notoriously difficult to determine especially if measurements of polarization are not available [*Knobelspiesse et al.*, 2012].

[16] Increased accuracy in the determination of the total optical thickness from glint observations stems only in part from a better estimate of absorption. Regarding the long-standing question concerning the Single-Scattering Albedo (SSA), the detectable improvement (~ 0.01) observed for moderate AOTs of the absorbing MI aerosol (solid lines) degrades at high AOTs. The larger improvement for the LH aerosol is deceptive, since this aerosol type is minimally absorbing. The same argument is valid for the imaginary part of the refractive index of the fine mode from which the SSA is derived.

[17] The relative magnitude of the uncertainties for the parameters linked to the coarse mode of the two aerosol models is not surprising, because for the MI type the fraction of this mode is much smaller. When the coarse mode load is significant, these uncertainties can be greatly reduced by including channels in the SWIR.

[18] An accurate retrieval of the wind speed clearly depends on the availability of a glint profile to fit the Cox-Munk model (i.e., it benefits from scans oriented closely to the principal plane) and degrades at higher AODs because the sunglint patch becomes partly obscured. The same reasoning applies
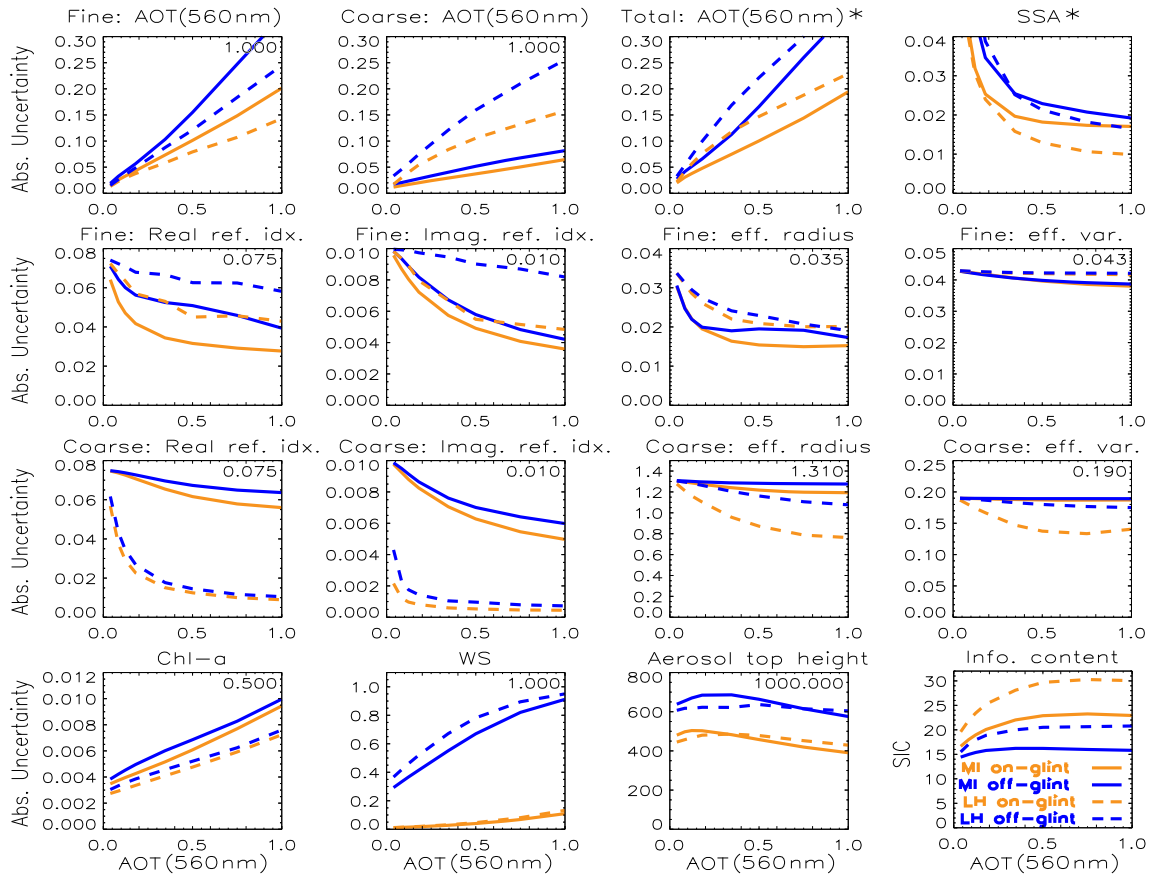

Figure 1. Simulated absolute uncertainties (except for the bottom-right panel, representing the SIC) as a function of optical thickness for the retrieval of relevant parameters of non-absorbing Lanai (LH, dashed lines) and absorbing Maldives (MI, solid lines) maritime aerosols (see Table 1). Results from observations within the glint are in orange, and those from off-glint scans in blue. At the top-right corner of each panel is the a priori value for the relative parameter. The asterisk indicates a derived parameter, not directly retrieved, and for which the uncertainty is calculated using the uncertainties in its constituent parts.

to the determination of the chlorophyll concentration from the isolation of the water leaving radiance contribution, i.e., the atmospheric correction is more accurate at low optical thicknesses. Moreover, in this case the in-glint and off-glint results nearly overlap since the glint is an interface effect that has no influence on the underwater field (provided that sufficient dynamical range is available). Although the sensitivity to the vertical distribution of aerosols is also improved, the uncertainty remains high ($\sim$50%), which confirms the challenges encountered by passive sensors in determining such a parameter, especially in the presence of absorption.

[19] A glance at the SIC suggests that glint measurements of moderate-to-high aerosol loads add 6 to 10 bits of information compared to off-glint observations, depending on the aerosol type. For the absorbing MI model, the measurement provides the capability of discerning up to $2^6 \sim 60$ additional states relative to the respective a priori number.

[20] The formalism employed here fully predicts the actual performance of a sensor only if all sources of measurement and model uncertainties are properly accounted for. The results quantify the sensitivity to parameter variability, but should not be taken as an absolute measure of parameter retrievability. Considering that the physics of the system cannot be perfectly captured by the forward model, and that sub-pixel variability is neglected, the uncertainties should be taken as underestimates. Moreover, the ideal form of the measurement error covariance matrix greatly depends on instrument-specific correlations. Nevertheless, the objective of this study is not affected by these limitations, since in- and off-glint observations differ exclusively in the strength of the illumination reflected by the surface.

4. Conclusions

[21] This work focused on sensitivity of simulated, remote sensing observations of tropospheric aerosols to absorption. The analysis pertains to maritime aerosol models compiled after AERONET measurements and supports the hypothesis of *Kaufman et al.* [2002] that the increased signal-to-noise ratio, obtained by scanning across the glint region, can indeed improve the retrieval of aerosol absorption. The effect is nevertheless moderate and is a consequence of the reduction in uncertainty of all descriptive parameters.

[22] We have chosen to model the prototype instrument for which the simulations are performed with characteristics similar to those of sensors already in orbit. It should be noted that the computed uncertainties undergo expected and very significant reductions by including channels in the SWIR and polarization capabilities. In the first case, improvements are noted mostly in the uncertainties relative to the aerosol coarse mode. In the case of polarization, it is clear that the exquisite sensitivity to particle microphysics benefits the retrieval of both fine and coarse aerosol parameters, to the extent that the presence or absence of the glint becomes nearly irrelevant.

References

Andreae, M. (2001), The dark side of aerosols, *Nature*, *409*, 671–672.
Bates, T., B. Lamb, A. Guenther, J. Dignon, and R. Stoiber (1992), Sulfur emissions to the atmosphere from natural sources, *J. Atmos. Chem.*, *14*, 315–337.
Chowdhary, J., B. Cairns, F. Waquet, K. Knobelspiesse, M. Ottaviani, J. Redemann, L. Travis, and M. Mishchenko (2012), Sensitivity of multiangle, multispectral polarimetric remote sensing over open oceans to water-leaving radiance: Analyses of RSP data acquired during the MILAGRO campaign, *Remote Sens. Environ.*, *118*, 284–308.
Coddington, O., P. Pilewskie, and T. Vukicevic (2012), The Shannon information content of hyperspectral shortwave cloud albedo measurements: Quantification and practical applications, *J. Geophys. Res.*, *117*(D04), 205, doi:10.1029/2011JD016771.
Cox, C., and W. Munk (1956), Slopes of the sea surface deduced from photographs of sun glitter, *Bull. Scripps Inst. Oceanogr.*, *6*, 401–488.
De Haan, J., P. Bosma, and J. Hovenier (1987), The adding method for multiple scattering calculations of polarized light, *Astron. Astrophys.*, *183*, 371–391.
Diner, D., et al. (1998), Multi-angle Imaging SpectroRadiometer (MISR) instrument description and experiment overview, *IEEE Trans. Geosci. Remote Sens.*, *36*, 1072–1087.
Dubovik, O., B. Holben, T. Eck, A. Smirnov, Y. Kaufman, M. King, D. Tanré, and I. Slutsker (2002), Variability of absorption and optical properties of key aerosol types observed in worldwide locations, *J. Atmospheric Sci.*, *59*, 590–608.
Hansen, J., M. Sato, P. Kharecha, and K. von Schuckmann (2011), Earth's energy imbalance and implications, *Atmos. Chem. Phys.*, *11*, 13,421–13,449, doi:10.5194/acp-11-13421-2011.
Hasekamp, O. (2010), Capability of multi-viewing-angle photo-polarimetric measurements for the simultaneous retrieval of aerosol and cloud properties, *Atmos. Meas. Tech.*, *3*, 839–851.
Hasekamp, O. P., and J. Landgraf (2007), Retrieval of aerosol properties over land surfaces: Capabilities of multiple-viewing-angle intensity and polarization measurements, *Appl. Opt.*, *46*, 3332–3344.
Holben, B., et al. (1998), AERONET–A federated instrument network and data archive for aerosol characterization, *Remote Sens. Environ.*, *66*, 1–16.
Kaufman, Y. J., J. V. Martins, L. Remer, M. R. Schoeberl, and M. A. Yamasoe (2002), Satellite retrieval of aerosol absorption over the oceans using sunglint, *Geophys. Res. Lett.*, *29*, 34–1, doi:10.1029/2002GL015403.
Kay, S., J. D. Hedley, and S. Lavender (2009), Sun glint correction of high and low spatial resolution images of aquatic scenes: A review of methods for visible and near-infrared wavelengths, *Remote Sens.*, *1*, 697–730.
Knobelspiesse, K., B. Cairns, M. Mishchenko, J. Chowdhary, K. Tsigaridis, B. van Diedenhoven, W. Martin, M. Ottaviani, and M. Alexandrov (2012), Analysis of fine-mode aerosol retrieval capabilities by different passive remote sensing instrument designs, *Opt. Express*, *20*, 21,457–21,484.
Knobelspiesse, K., B. Cairns, J. Redemann, R. Bergstrom, and A. Stohl (2011), Simultaneous retrieval of aerosol and cloud properties during the MILAGRO field campaign, *Atmos. Chem. Phys.*, *11*, 6245–6263.
Lebsock, M., T. L'Ecuyer, and G. Stephens (2007), Information content of near-infrared spaceborne multiangular polarization measurements for aerosol retrievals, *J. Geophys. Res.*, *112*(14), 206.
Loeb, N., and W. Su (2010), Direct aerosol radiative forcing uncertainty based on a radiative perturbation analysis, *J. Clim.*, *23*, 5288–5293.
Mishchenko, M., and L. Travis (1997), Satellite retrieval of aerosol properties over the ocean using polarization as well as intensity of reflected sunlight, *J. Geophys. Res.*, *102*, 16,989–17,013.
Moosmüller, H., R. Chakrabarty, and W. Arnott (2009), Aerosol light absorption and its measurement: A review, *J. Quant. Spectrosc. Radiat. Transfer*, *110*, 844–878.
Ottaviani, M., R. Spurr, K. Stamnes, W. Li, W. Su, and W. Wiscombe (2008), Improving the description of sunglint for accurate prediction of remotely sensed radiances, *J. Quant. Spectrosc. Radiat. Transfer*, *109*, 2364–2375.
Penner, J., L. Xu, and M. Wang (2011), Satellite methods underestimate indirect climate forcing by aerosols, *Proc. Natl. Acad. Sci.*, *108*, 13,404–13,408.
Rodgers, C. (2000), *Inverse Methods for Atmospheric Sounding Theory and Practice*, vol. 2 of *Series on Atmospheric, Oceanic and Planetary Physics*, World Scientific Publishing Company, Singapore.
Rodgers, C., and B. Connor (2003), Intercomparison of remote sounding instruments, *J. Geophys. Res.*, *108*, 4116, doi:10.1029/2002JD002299.
Seinfeld, J. H., S. N. Pandis, and K. Noone (1998), Atmospheric chemistry and physics: From air pollution to climate change, *Phys. Today*, *51*, 88.
Smith, S., H. Pitcher, and T. Wigley (2001), Global and regional anthropogenic sulfur dioxide emissions, *Global Planet. Change*, *29*, 99–119.
Tanré, D., et al. (2011), Remote sensing of aerosols by using polarized, directional and spectral measurements within the A-Train: The PARASOL mission, *Atmos. Meas. Tech.*, *4*, 1383–1395.
Wagner, R., T. Ajtai, K. Kandler, K. Lieke, C. Linke, T. Müller, M. Schnaiter, and M. Vragel (2012), Complex refractive indices of Saharan dust samples at visible and near UV wavelengths: A laboratory study, *Atmos. Chem. Phys.*, *12*, 2491–2512.
Waquet, F., B. Cairns, K. Knobelspiesse, J. Chowdhary, L. Travis, B. Schmid, and M. Mishchenko (2009), Polarimetric remote sensing of aerosols over land, *J. Geophys. Res.*, *114*(D01), 206–228, doi:10.1029/2008JD010619.